The ultraviolet and vacuum ultraviolet absorption spectrum of gamma-pyrone; the singlet states studied by configuration interaction and density functional calculations.

Michael H. Palmer,[1,a] Søren Vrønning Hoffmann,[2,b] Nykola C. Jones,[2,b] Marcello Coreno,[3,b] Monica de Simone,[4,b] Cesare Grazioli.[4,b] R. Alan Aitken,[5,b] Loëlia Perrault[5,b] and Iain L. J. Patterson.[5,b]

[1] *School of Chemistry, University of Edinburgh, Joseph Black Building, David Brewster Road, Edinburgh EH9 3FJ, Scotland, UK*3
[2] *ISA, Department of Physics and Astronomy, Aarhus University, Ny Munkegade 120, DK-8000, Aarhus C, Denmark*
[3] *ISM-CNR, Instituto di Struttura della Materia, LD2 Unit 34149 Trieste, Italy*
[4] *IOM-CNR, Istituto Officina dei Materiali, Basovizza SS-14, Km 163.5, 34149 Trieste, Italy*
[5] *School of Chemistry, University of St Andrews, North Haugh, St Andrews, Fife, KY16 9ST, Scotland, UK (United Kingdom).*
[a)] Email: *m.h.palmer@ed.ac.uk*:
[b)] Electronic addresses:
vronning@phys.au.dk; nykj@phys.au.dk; *marcello.coreno@elettra.eu; desimone@iom.cnr.it; grazioli@iom.cnr.it; raa@st-andrews.ac.uk; loelia.prt@gmail.com; iljp@st-andrews.ac.uk*

ABSTRACT

A synchrotron based vacuum ultraviolet absorption spectrum for γ-pyrone has been interpreted in terms of singlet excited electronic states, using a variety of coupled cluster, configuration interaction, and density functional calculations. The extremely weak spectral onset at 3.557 eV shows 8 vibrational peaks and following previous analyses is attributed to a forbidden $^1A_2$ state. A contrasting broad peak with maximum at 5.381 eV has a relatively high cross-section of 30 Mb; this arises from three overlapping states, where a $^1A_1$ state dominates over progressively weaker $^1B_2$ and $^1B_1$ states. After fitting the second band to a polynomial Gaussian function, and plotting the regular residuals (RR), over 20 vibrational peaks were revealed. We have had limited success in analyzing this fine structure. However, the small separation between these three states clearly shows that their vibrational satellites must overlap. Singlet valence and Rydberg state vibrational profiles were determined by configuration interaction using the CAM-B3LYP density functional. Vibrational analysis, using both Franck-Condon

and Herzberg-Teller procedures showed that both procedures contributed to the profiles. Theoretical Rydberg states were evaluated by a highly focused CI procedure. Super-position of the lowest photoelectron spectral band on the VUV spectrum near 6.4 eV, shows that the 3s and 3p Rydberg states based on the $^2B_2$ ionic state are present; those based on the other low-lying ionic state (X^2B_1) are destroyed by broadening; this is a dramatic extension of the broadening previously witnessed in our studies of halogenobenzenes.

I. INTRODUCTION

Recently we reported a synchrotron-based redetermination of the photoionization spectrum for γ-pyrone,[1] a substance systematically described as 4H-pyran-4-one. The fully conjugated ring system depicted in Figure 1 as structure ***1a,*** has raised the issue of whether the system is aromatic, and also whether it supports a ring current.[2] Several studies by nuclear magnetic resonance (NMR)[2-7] and microwave spectroscopy (MW),[8-12] have been performed in order to address these subjects and were discussed in reference 1. The detailed structure derived from the MW studies, shows that the observed bond lengths support the classical formulation as in 1a, while the reactivity and substantial dipole moment point,[10] 3.79 ± 0.02D,[10] point to contributions of structure 1b. Further, the C_2=C_3 double bond measured by MW spectroscopy is 1.344 Å, almost the same as that for ethylene (1.339 Å), while the C_3 – C_4 single bond at 1.463 Å is very close to cyclopentadiene (1.469 Å); the C_4 = O_4 double bond at 1.226 Å is also very similar to that for acetone (1.222 Å).[10]

Figure 1. Representations of the structure of γ-pyrone are shown in 1a and 1b; the high dipole moment is expressed by 1b, whereas the bond-lengths as measured by microwave spectroscopy are close to those of the classical representation 1a.

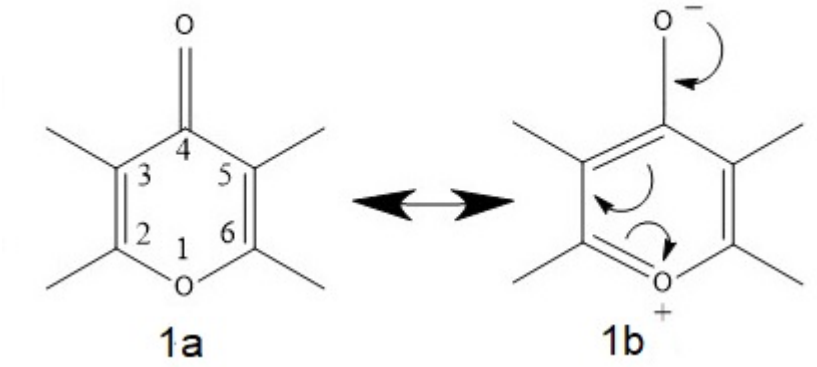

The vibrationally averaged nematic phase γ-pyrone structures determined from ^{1}H and ^{13}C NMR spectroscopy are also in close agreement with the MW results.[13,14,15] Magnetic susceptibility anisotropies, analysed by MW spectroscopy in terms of local and non-local contributions, show that both γ-pyrone and the related lactone (α-pyrone), have negligibly small non-local contributions; thus both are considered to be non-aromatic by this magnetic criterion. Theoretical results, near Hartree-Fock in quality for magnetic susceptibilities, and comparison with experimental values also seem to indicate that the 2- and 4-pyrones are non-aromatic.[16] Fully optimised ab initio calculations on 4H-pyran-4-one (1a) and its three sulphur analogues, where one or both O-atoms are exchanged by S-atoms, and determination of the electrostatic potentials in four planes around the molecule, leads to the conclusion that all four molecules are essentially non-aromatic.[17]

We now report a synchrotron-based study of the UV + VUV (vacuum ultraviolet) absorption spectrum for γ-pyrone, in the energy range 3.344 to 10.78 eV, following our recent studies of azulene and other fully conjugated molecules.[18,19] In the current study, we will use energy units of electron volts (eV) and wave-number (cm^{-1}), but will refer to other units when used by other authors. There is a considerable body of information concerning the UV absorption of γ-pyrone.[20,21,22] This band lies close to the long-wavelength limit of our synchrotron spectrum,

shown in black in Figure 2. We have obtained the UV spectrum with a standard laboratory instrument, superimposed in blue. These two procedures provide an independent measurement for that energy region.

Figure 2. The wide scan from the synchrotron absorption in the vapour phase, combined with the ultraviolet spectral results (shown in blue) for γ-pyrone in cyclohexane solution.

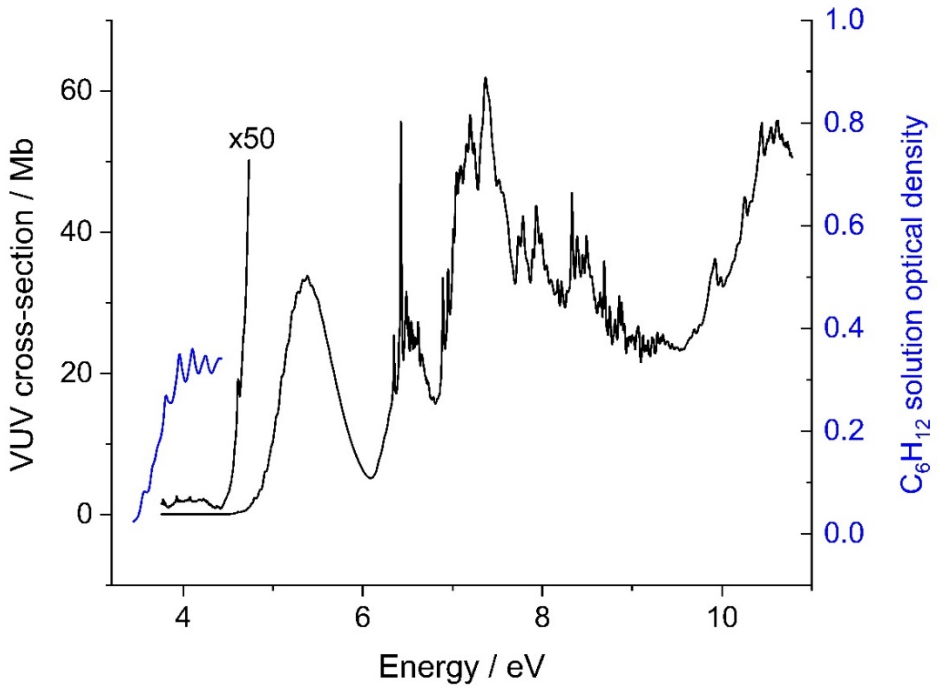

The UV absorption, conventionally denoted as the $S_1(n\pi^*)$ transition, was originally assigned to the forbidden $^1A_2$ $n\pi^*$ state, as a set of 8-maxima with λ_{max} 248 nm, and electronic origin close to 3.516 eV.[22] This S_1 band, spin-allowed but orbitally forbidden,[23] was thought to gain oscillator strength through vibronic mixing with $S_2(\pi\pi^*)$ or higher singlet $\pi\pi^*$ excited states. CRD spectroscopy of phosphorescence by the lowest lying $n\pi^*$ T_1 state, has led to detailed analysis[24] of the 0^0 band origin as 3.384 eV. However, a supersonic free-jet expansion, where jet cooling eliminated congestion, led to a revised analysis.[25] An important conclusion was that time-dependent density functional theory (TDDFT), using the PBE0 functional gave more realistic vibration frequencies than the more computationally demanding equation of motion

with coupled cluster singles doubles (EOM-EE-CCSD) method.[25] We will use the TDDFT method together with the CAM-B3LYP functional in the present study, as described in the Methods section below.

Under the influence of UV light, and under high concentration, 4H-pyran-4-ones with phenyl substituents at C_3 and C_5 undergo dimerization to "head-to-tail" dimers, which are 2H-pyran-2-ones;[26] conversely, high dilution inhibits dimerization. The formation of pyran-2-ones from 4-ones with C_{2V} ring skeletons, requires an unsymmetrical intermediate state; thus non-planar structures were also considered for singlet excited states of γ-pyrone.[26] This was abandoned when it became clear that the bulky C_3 or C_5 substituents must be responsible for the necessary twisting of the ring structure to occur.

II. METHODS

Following our previous study,[1] the γ-pyrone sample, CAS registry number 108-97-4, was synthesized by standard methods,[27,28,] and the purity checked by ^1H and ^{13}C nuclear magnetic resonance before use.

(a) The spectral study

This was performed on different instruments for different energy regions. (i) *Measurements in solution.*

The UV spectrum of γ-pyrone in the region of 280 to 360 nm (4.428 to 3.444 eV) was measured on a Shimadzu UV1600 instrument, using a 10 cm path length cell at a concentration of 2.08 g/L in cyclohexane; the 402 data points were separated by 0.2 nm. Insufficient vapour pressure precluded acquisition of the gas phase spectrum above 290 nm. The resulting spectrum is shown in blue in Figure 2.

(ii) Gas phase measurements

The VUV-UV spectrum of γ-pyrone, shown in Figure 2, was measured at 30°C in the range 115 to 330 nm (10.78 to 3.757 eV) using the AU-UV beam line on the ASTRID2 synchrotron

light source at the Department of Physics and Astronomy, Aarhus University, Denmark.[29] The setup used to measure this spectrum of γ-pyrone has been described in detail in a previous publication,[29] so only a brief summary will be given here. The AU-UV beam line, which takes light from a dipole magnet in ASTRID2, provides monochromatic light with a resolution of 0.08 nm, using a 2000 lines/mm toroidal grating and 100-micron entrance and exit slits. A gas cell enclosed with MgF_2 windows on the entrance and exit, is mounted on the exit port of the beam line and evacuated using a turbo pump. The intensity of light passing through the cell over a range of wavelengths is measured using a photomultiplier tube on the exit of the cell, with and without the sample gas. The pressure in the cell is monitored using a heated 1 Torr capacitance manometer, with pressures chosen to ensure that attenuation of the incident light is low enough to avoid line saturation (typically 50% or less). Absolute photoabsorption cross-sections are then calculated using the known path length, l = 15.5 cm, of the cell using the Beer-Lambert Law $I_t = I_0 \exp(-N\sigma l)$, where I_0 is the incident light intensity, I_t is that transmitted with the gas in the cell and N the molecular number density determined from the pressure. Small sections of the spectrum are recorded with overlap, choosing the optimum pressure for the cross-section for each region, to ensure that it is being measured without saturation effects. The beam current in the ASTRID2 light source, which runs in "top-up" mode, is continuously monitored, and the light intensity recorded by the photomultiplier is normalised to remove effects of the decaying beam and injections.

(b) Theoretical methods

Our study necessitates use of several codes, since no individual computational chemistry suite contains all the modules needed. The most inclusive is Gaussian Inc. version G-16,[30] which also contains the symmetry adapted cluster (SAC) configuration interaction code (CI),[31-35] the vibrational analysis code originally from Pisa,[36-38] and the time-dependent density functional theory (TDDFT) code.[39-41] The principal functional used in this study was a long-range-

corrected version of the Becke 3-parameter hybrid functional (B3LYP),[42] described as the Coulomb-attenuating method (CAM-B3LYP).[43] Excited state adiabatic excitation energy (AEE) determination was carried out within TDDFT; this enabled equilibrium structures and harmonic frequencies for both valence and Rydberg states to be determined, and Franck-Condon (FC) and Herzberg-Teller (HT) vibrational analyses to be performed on the resulting wave-functions. Vertical excitation energies (VEEs) were also determined by use of the MRD-CI method[44] in GAMESS-UK;[45] a description of this method is included in the Supplementary Material as SM1.

(c) The principal basis sets

Atomic basis sets developed in recent years attempt to cover all types of excited state, with universal bases containing extremely high Gaussian exponents for states close to the nuclei, and diffuse (exceptionally low exponents) for Rydberg states. We find it appropriate to treat these two types of state separately as in our recent studies.[19,46] We used triple-zeta valence with single polarization in all cases; this included using the 6-311G (d, p) basis set[47] in conjunction with the SAC-CI module[31-35] of GAUSSIAN (G-16), and TZVP[48] with MRD-CI[44] of GAMESS-UK.[45] TDDFT is a single-configuration process; the excited state structure, determined theoretically, is used for both the ground and excited state. The potential energy surface in spectroscopy relies on differences between the potential energies of both upper and lower states at their equilibrium structures; we have introduced this correction when the vibrational states and their intensities are determined by the Pisa software. The results were subsequently enhanced by using the MRD-CI method.

III. RESULTS AND DISCUSSION

The X^1A_1 electronic state of γ-pyrone has C_{2V} symmetry[8,9,10] with 25 doubly occupied molecular orbitals (DOMOs); 7 of these represent the core O_{1s}^2 and C_{1s}^2 electrons ($5a_1^2 + 2b_2^2$).

Throughout this study, we will use valence shell labelling for the doubly occupied molecular orbitals (DOMOs), which are: $1a_1$ to $8a_1$, $1b_1$ to $3b_1$, $1b_2$ to $6b_2$ and $1a_2$.

(A).The theoretical γ-pyrone UV +VUV absorption spectrum.

The theoretical manifold contains both valence and Rydberg states; the profiles for these states are shown separately in Figures 3 and 4, respectively. This is complex, owing to a wide intensity range with some broad bands, and sharp structure with close similarity to that of the photoelectron spectrum.[1] Semi-empirical calculations[48] of the lower singlet states for γ-pyrone, suggest that the nπ* state is lower in energy than ππ* by ~2000 cm^{-1} (0.248 eV).[48] Our study, shown in Table I, clearly shows the onset of the spectrum has four states, namely $^1A_2$ << $^1B_2$ < $^1B_1$ < $^1A_1$; these have widely different intensities, which are zero, medium, low and very intense. We accept the proposition[24] that the forbidden $^1A_2$ state gains intensity by borrowing from the overlapping group of three states.

Figure 3. The valence state vertical excitation energies for the singlet states, using the MRD-CI method and the TZVP basis set. The calculated energies, shown in red, are unscaled. There are 3 nearly degenerate states under the envelope between 5 and 6 eV; these are: $^1A_1$ (strong) < $^1B_2$ < $^1B_1$ which are both weak. Sharp vibrational structure is apparent in the peak close to 6.5 eV and must be attributed to Rydberg states, as described below.

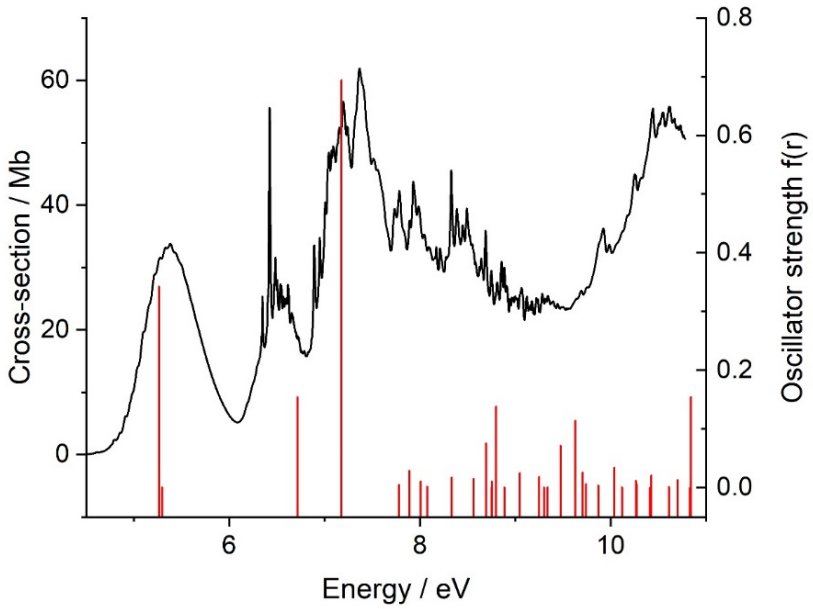

A principal objective of this study is to interpret the observed bands in the UV + VUV absorption spectrum over a wide range of vertical excitation energies (VEE); these are shown in Table I. The valence states will form the basis of the most intense absorption, while fine structure previously analysed in the photoelectron spectrum, will be present in the corresponding Rydberg states in absorption. We discuss these two types of absorption separately, but first consider the effect of change of theoretical method on the excitation energies observed; this enables common features to be identified.

Figure 4. The s-Rydberg states for $^1B_1$, $^1B_2$ and $^1A_1$ symmetries, are shown in blue, red, and magenta, respectively. The oscillator strengths have been increased by 0.05 units, to make them more distinct. The states shown are from calculations where both valence and Rydberg functions are present, and thus allow interactions between these two types of excited state.

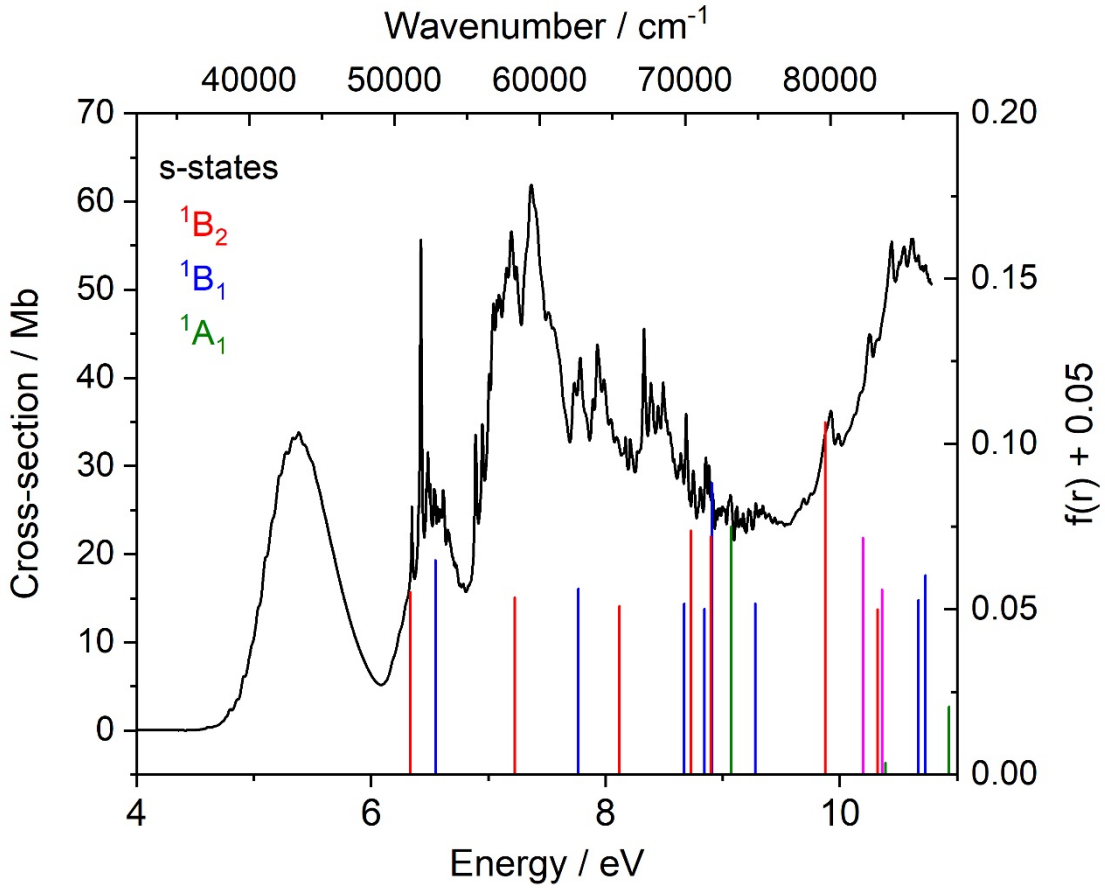

Table I. The valence states of γ-pyrone determined by the MRD-CI method together with the TZVP basis set. The lowest excited state, but not optically allowed, is $^1A_2$ at 3.952 eV. Where more than one term is shown, the density decreases from left to right both in this and related Tables. For example: the lowest allowed ($^1A_1$) state has densities 0.894 and –

0.263; it is coupled to the second $^1B_2$ state, which has also two leading terms, with densities 0.921 and -0.173.

Energy / eV	Oscillator strength	Symmetry	Leading terms
3.952	0.0	A_2	$3b_1 6b_2$*
5.243	0.346	A_1	$3b_1 4b_1^*$ - $1a_2 2a_2$*
5.266	0.014	B_2	$3b_1 2a_2$*
5.298	0.000	B_1	$6b_2 2a_2$*
6.716	0.154	B_2	$1a_2 4b_1$*- $3b_1 2a_2$*
7.063	0.646	A_1	$1a_2 2a_2$*+ $3b_1 4b_1^*$
7.640	0.017	A_1	$6b_2 7b_2$*
7.780	0.005	B_2	$6b_2 9a_1$*
7.790	0.011	A_1	$2b_1 4b_1$* + $3b_1^0 4b_1$*^{2}
7.840	0.028	B_1	$3b_1 9a_1$*
8.054	0.002	B_1	$8a_1 4b_1$*
8.149	0.014	A_1	$3b_1 5b_1$* - $2b_1 4b_1$*
8.692	0.075	B_2	$6b_2 10a_1$* + $6b_2 12a_1$*
8.710	0.002	B_1	$5b_2 2a_2$ - $7a_1 4b_1$*
8.737	0.001	B_1	$3b_1 11a_1$* + $3b_1 10a_1$*
8.753	0.010	B_2	$6b_2 11a_1$* - $6b_2 12a_1$*
8.798	0.138	B_2	$2b_1 2a_2$*
9.219	0.018	B_1	$3b_1 10a_1$* - $3b_1 11a_1$*
9.339	0.000	B_2	$1a_2 5b_1$* + $3b_1 3a_2$*
9.474	0.071	B_2	$1a_2 6b_1$* + $1a_2 5b_1$* -$3b_1 3a_2$*
9.591	0.022	A_1	$6b_2 8b_2$* + $2b_1 5b_1$*
9.657	0.131	A_1	$6b_2 9b_2$*
9.694	0.018	B_1	$1a_2 7b_2$*+ $5b_2 2a_2$*
9.862	0.007	B_1	$7a_1 4b_1$*
10.115	0.020	B_1	$3b_1 12a_1$*
10.124	0.011	A_1	$8a_1 9a_1$*
10.277	0.013	A_1	$3b_1 7b_1$*
10.407	0.000	B_2	$3b_1 3a_2$* - $1a_2 6b_1$* - $1b_1 2a_2$*
10.672	0.135	B_1	$3b_1 13a_1$*
10.746	0.041	B_1	$3b_1 14a_1$*

(B). Change in vertical excitation energies (VEE) with theoretical method.

The SAC-CI study, our most rigorous procedure, was performed at the equilibrium structure of the X^1A_1 state for γ-pyrone, leading to predictions for the VEE of the excited states. The TDDFT method using the CAM-B3LYP functional generated the equilibrium structure for all the low-lying states. Since G-16 determines the adiabatic excitation energy (AEE) for both ground and excited state at the excited state structure, rather than the spectroscopic method

where ground and excited state structures are independently determined at their equilibrium structures. Hence we make a correction to the computed AEE to conform to the spectroscopic definition.

We find a very tight correlation between these SAC-CI state energies with those from the TDDFT method. On a like-for-like symmetry comparison, i.e. A_1 with A_1, B_1 with B_1, B_2 with B_2, and A_2 with A_2, we find the correlation for the combined sets is CAM = 0.890(13)*SAC + 0.562(145), where CAM and SAC are abbreviations for the energies using the respective methods; standard errors are in parentheses. For the range of states up to 10.0 eV VEE, the mean difference is 0.360 eV, while the maximum difference is 0.705 eV. The correlation is shown in the supplementary material under SM2. Recently we observed a very similar correlation between SAC-CI and CAM-B3LYP energies for singlet states of quadricyclane.[46] Since these two methods have a very different demand on computing resources, this enables us to concentrate on the CAM-B3LYP at equilibrium much more cheaply; further, the TDDFT wave-functions are compatible with the Franck-Condon and Herzberg-Teller vibrational suite. In contrast, the SAC-CI suite is limited to providing information about the energy and oscillator strength of states.

A correlation between MRD-CI and the SAC-CI energy results, yielded MRD = 0.972(38)*SAC + 0.645(378), where MRD is the abbreviation used for the MRD-CI methods; standard errors are in parentheses. The scatter between the SAC-CI and MRD-CI results is slightly larger, but the saving in CPU-time is even larger than with CAM-B3LYP. Overall, these equations show that there is a close excitation energy relationship between the methods, and the correlation with experiment could be performed with each; in the following Sections we use the MRD-CI as examples.

(C). The valence shell singlet states.

The highest occupied orbitals contain both π and lone pair σ-orbitals. All the excitations shown in Table I, are from the 5-highest occupied MOs, and most are excited into one of the 5-lowest VMOs. The group of highest occupied and lowest unoccupied MOs are shown in Figure 5. The lowest configurations leading to excited states with high oscillator strength are ππ* states. Some of those shown in Table I have more than one leading configuration, and there the dominant configuration is the first mentioned. As noted above, there are grounds for accepting that the $^1A_2$ state, classically forbidden in absorption, mixes with adjacent allowed states. The next three lowest excited states lie within 0.1 eV in energy but have significant differences in intensities.

All three states will exhibit vibrational structure, so that these vibrations will clearly overlap each other, leading to extensive mixing of states of different symmetry. We are unable to evaluate these mixed states, so our interpretation of the observed spectrum will be limited; although much vibrational structure has been identified; this must await later study. When we superimpose the classical profile, without mixing of states, on the experimental UV + VUV absorption spectrum, as in Figure 3, only perturbed levels from the highest oscillator strength band will be apparent, with the second and third states either very weak or absent. Overall, most of the theoretical oscillator strength is limited to B_2 and A_1 symmetry states, and these must be correlated with the observed spectral intensity.

Several symmetric and antisymmetric combinations of ππ* excitations occur; for the $3b_14b_1^*$ ± $1a_22a_2$* pair of states the separation is 1.82 eV, with the symmetric state lies at lower energy. These two states have the highest oscillator strengths of the calculated levels. Not only ππ* states occur as linear combinations; the πσ* ($^1B_1$) pair $3b_111a_1^*$ ± $3b_110a_1^*$ are separated by 0.48 eV. Further details of these results are given in the supplementary material under SM3, which also contains a full set of roots, together with their oscillator strengths and second moments of the charge distribution (SECMOM). The latter give a direct measure of the spatial

volume of the natural orbitals. Valence states have values for the operators $\langle x^2 \rangle$, $\langle y^2 \rangle$ and $\langle z^2 \rangle$ close to those of the X^1A_1 ground state, which are -31.3, -24.0 and -36.8 a.u. respectively. These operators lead to markedly larger magnitudes for Rydberg states, some of which are shown below. Limited valence shell results using the coupled cluster method (SAC-CI), are shown in the supplementary material as SM4.

(D). Vibrational analysis of the valence states.

The complete assignment of the vibrational spectroscopy of γ-pyrone ground state, including potential energy distributions, has been studied in detail, including matrix-isolation in an argon matrix and Fourier-transform infrared spectroscopy.[49a,b] A comparison of the harmonic frequencies for the X^1A_1 with the 4 lowest electronically excited valence states is shown in Table II. The present X^1A_1 results give a very close correlation with the Ar matrix data of Fausto et al,[49a] namely: $\nu_{Calc} = 1.063(7) - 34\ (11)$ with correlation coefficient (adjacent R^2) 0.999. This includes the ν(C-H) stretching vibrations, where the difference averages at 172 cm^{-1}; if these are excluded, the median difference between theory and experiment is 26 cm^{-1}. This correlation gives confidence that the values for the excited states in Table II are realistic. Further, that the nature of the vibrations follows the PED analysis. Fausto et al,[49a] give an even closer correlation between their Hartree-Fock 6-31G* calculation with the Ar matrix values, but all their frequencies were subjected to a single scaling factor of 0.89. This was performed under both Franck-Condon (FC) and Herzberg-Teller (HT) selection rules, since it was found that for each of the lowest group of valence states, the contributions from each regime cannot be ignored. In practice, it was found that the combined function, FCHT, in G-16 was best, since it enforces a common intensity scale. In each case C_{2V} symmetry was enforced, but clearly these are saddle points for some states, where a single negative eigenvalue was obtained. We have been unable to complete a more sophisticated approach to get beyond this situation satisfactorily.

Table II. Energies and harmonic frequencies for the X^1A_1 ground state and lowest valence excited valence states using the TDDFT methods.

Root	0	1	2	3	4
	X^1A_1	$^1A_2$	$^1B_1$	$^1B_2$	$^1A_1$
Energy /a.u.	-343.28918	-343.14303	-343.09838	-343.09256	-343.07413
Oscillator strength	0	0.0	0.0000	0.0158	0.2043
Frequencies / cm^{-1}					
Mode and symmetry					
1 (A1)	3246	3265	3298	3284	3269
2	3225	3234	3270	3267	3225
3	1794	1689	1565	1542	1553
4	1716	1223	1477	1444	1441
5	1434	478	1383	1348	1318
6	1224	1441	1214	1177	1164
7	1031	1372	1061	1033	1004
8	953	1018	943	957	918
9	820	812	868	859	790
10	509	930	497	512	477
11(A2)	1003	922	597	719	798
12	837	753	326	554	618
13	410	434	-251	112	295
14(B1)	997	911	687	735	843
15	882	719	652	660	566
16	749	577	577	600	484
17	449	268	505	505	281
18	158	140	176	197	-140
19 (B2)	3243	3259	3292	3269	3342
20	3225	3233	3288	3262	3224
21	1650	1591	2225	1419	2593
22	1446	1365	1428	1286	1380
23	1355	1271	1376	1228	1265
24	1238	1131	1282	1144	1051
25	1052	951	974	784	727
26	653	673	611	615	466
27	463	353	407	-232	330

The FCHT analyses for the lowest three states, $^1A_1$, $^1B_2$ and $^1B_1$ are shown in Tables III, IV and V; the intensities vary dramatically, both for the 0-0 bands and the vibrational satellites, at both the FC and HT levels. Since future studies may include state symmetry specific determination, we give the most intense vibrations for each state; to make sure the HT manifold is shown, we adjust the criteria for intensity between FC and HT states. Given the small separations in energy, all three vibrational sequences will overlap, and the issue of visibility in the experimental spectrum will be the result of both the intensities of the separate vibrational

states, and any perturbations arising from interactions between states. The separate states clearly indicate the visibility in the spectrum should be $1^1A_1 > 1^1B_2 >> 1^1B_1$.

The principal vibrations stimulated in the 1^1A_1 valence state in the Franck-Condon mode are the usual types of single quanta of a_1-fundamentals, and even quanta of non-symmetric modes, as well as binary and higher combination bands, as shown in Table IV. The 0-0 band is intense, and only the a_1-fundamentals 790 and 918 cm^{-1} are present, both with exceedingly high intensity. In the HT profile, more fundamentals are prominent, namely 329, 467, 727, 1004, 1164, 1318 and 1441 cm^{-1}, but all are close to only 1% of the intensity of the two FC fundamentals.

Table III. Franck-Condon vibrational analysis of the $^1A_1$ valence state (4th root) at the CAM-B3LYP level of valence states using the 6-311G(d,p) basis set. Energy of the 0-0 transition: 46094 cm^{-1} = 5.715 eV. All theoretical intensities are given as molar absorption coefficients ($dm^3.mol^{-1}.cm^{-1}$) in this study.

Energy/cm^{-1}	Vibrational state	Intensity	Energy/cm^{-1}	Vibrational state	Intensity
0	0	321100	778	$6^1;1^4$	500
151	1^2	29250	790	11^1	37890
302	1^4	6096	793	$8^1;1^3$	1020
404	$3^1;1^1$	10460	796	$5^1;4^1$	6470
452	1^6	1382	809	$3^2;1^2$	1070
477	6^1	18800	809	$4^2;1^2$	4480
555	$3^1;1^3$	4181	829	$7^1;3^1$	291
575	$7^1;1^1$	581	857	$3^1;1^7$	407
594	2^2	4816	881	$6^1;3^1;1^1$	814
603	1^8	322	896	$8^1;3^1$	13620
628	$6^1;1^2$	2529	916	$9^1;2^1$	620
643	$8^1;1^1$	2632	918	14^1	27990
658	3^2	1073	933	5^2	815
659	4^2	34590	940	$11^1;1^2$	5168
706	$3^1;1^5$	1364	944	$8^1;1^5$	323
726	$7^1;1^3$	244	947	$5^1;4^1;1^2$	321100
745	$2^2;1^2$	617	959	$3^2;1^4$	29250

Table IV. Vibrational analysis of the $^1B_2$ valence state (3rd root) at the CAM-B3LYP level of valence states using the 6-311G(d,p) basis set. Energy of the 0-0 transition: 41759 cm^{-1} = 5.177 eV

(a)Franck-Condon

Energy/cm^{-1}	Vibrational state	Intensity	Energy/cm^{-1}	Vibrational state	Intensity
0	0	4251	1108	5^2	41
224	1^2	799	1115	$5^1;1^5$	9
393	2^2	6	1122	1^{10}	8
449	1^4	225	1165	$8^1;3^1$	23
512	4^1	1411	1177	16^1	3716
666	$5^1;1^1$	37	1178	$5^1;4^1;1^1$	12
673	1^6	70	1186	$4^1;1^6$	23
737	$4^1;1^2$	265	1229	7^2	2
797	$6^1;2^1$	102	1245	$6^1;2^1;1^4$	5
831	$9^1;1^1$	11	1249	$4^2;1^2$	44
857	$8^1;2^1$	11	1257	$14^1;1^2$	472
859	12^1	187	1260	$8^1;6^1$	12
891	$5^1;1^3$	20	1273	$9^1;5^1$	5
898	1^8	23	1280	$9^1;1^5$	3
906	$4^1;2^2$	2	1308	$12^1;1^4$	9
961	$4^1;1^4$	74	1309	$6^1;4^1;2^1$	33
1009	3^2	2	1320	8^2	54
1021	$6^1;2^1;1^2$	19	1329	$6^1;3^1;1^2$	11
1024	4^2	235	1332	$5^2;1^2$	11
1033	14^1	2524	1335	$10^1;6^1$	5
1055	$9^1;1^3$	6	1340	$5^1;1^7$	4
1081	$8^1;2^1;1^2$	2	1343	$9^1;4^1;1^1$	4
1084	$12^1;1^2$	34	1347	1^{12}	3
1104	$6^1;3^1$	56	1348	19^1	391

Table V. Vibrational analysis of the $^1B_1$ valence state (3rd root) at the CAM-B3LYP level of valence states using the 6-311G(d,p) basis set. Energy of the 0-0 transition: 41188 cm^{-1} = 5.107 eV

Energy/cm^{-1}	Vibrational state	Intensity	Energy/cm^{-1}	Vibrational state	Intensity
0	0	2	1383	10^2	0.508
497	4^1	1.126	1477	20^1	0.627
653	2^2	0.1	1558	$14^1;4^1$	0.197
681	$5^1;1^1$	0.07	1565	21^1	1.573
815	3^2	0.004	1711	$15^1;4^1$	0.572
862	$10^1;1^1$	0.007	1880	$18^1;4^1$	0.426
994	4^2	0.308	1974	$20^1;4^1$	0.344
1010	5^2	0.009	2062	$21^1;4^1$	0.862
1061	14^1	0.325	2208	$15^1;4^2$	0.231
1082	$6^1;5^1$	0.189	2218	$21^1;2^2$	0.118
1150	$4^1;2^2$	0.352	2275	$15^1;14^1$	0.236
1214	15^1	1.079	2429	15^2	0.444
1228	$9^1;6^1$	0.997	2444	$16^1;14^1$	0.113
1303	9^2	0.753	2539	$20^1;14^1$	0.141
1306	2^4	0.122	2559	$21^1;4^2$	0.222
1359	$10^1;4^1;1^1$	0.366			

The principal fundamentals in the Franck-Condon profile of the $^1B_2$ state of γ-pyrone are 512, 859, 1033 and 1177cm^{-1}; their intensities are high in relation to the corresponding combination bands, but markedly lower than the fundamentals in the 1^1A_1 state. This especially includes the 0-0 band. Several fundamentals appear in the 1^1B_2 state under Herzberg-Teller conditions, but these are even weaker. The Franck-Condon profile for the 1^1B_1 state is remarkably weak, but are reported with high precision, in the hope that spectroscopically focussed research on the 1^1B_1 state can extract these vibrations from the more intense states in this region. The fundamental FC vibrations are at 497, 1061, 1214 and 1565 cm^{-1}. The Herzberg-Teller fundamental vibrations are more intense than the Franck-Condon ones.

(E)The calculated Rydberg state profile.

After tests at various positions using the MRD-CI method,[46] the very diffuse Rydberg state functions (Gaussian functions, GTOs) were placed, together with the standard atomic basis functions, on the carbonyl O-atom. The calculations were done twice; once with only the valence state orbitals present, the second with the Rydberg functions added. The new MOs

are Rydberg states, within the valence set, by comparison of eigenvalues and density matrix. There is a high density of states, as shown by visually combining the theoretical states in Figures 3, 4 and 9. In the combined series, none of the eigenvalues are identical to those with only valence orbitals present. Thus each of the Rydberg states will inevitably be close to either a valence or Rydberg state enabling interactions. Similarly, the complex set of nuclei will provide an uneven attractive force towards the Rydberg electron. All these factors will reduce the usual near spherical symmetry of the electron distribution for the s-Rydberg states.

The energies of the calculated Rydberg 3s, 4s and 5s-states are shown in Table VI. All the extrapolated energies to the vertical ionization energy are low; the amounts are variable, but for the 4 lowest VIE lie between ±0.5 eV of the experimental ones. When Cartesian functions are used for d- and f-functions, the 6d→ 5d and 10f → 7f conversion to spherical harmonics are handled by the 'harmonic' directive in GAMESS-UK,[45] for the removal of the implicit s- and p-functions in 6d and 10f.

The principal s-Rydberg state energies are depicted in Figure 4, where different colours are used for B_1, B_2 and A_1 states. Similar diagrams can be drawn for the p-, d- and f-states, as previously reported for quadricyclane.[46] It is clear from Figure 4, that no Rydberg states lie under the spectral envelope below an excitation energy of 6 eV; thus, the broad band close to 5.5 eV can only contain valence states. In contrast, the two Rydberg s-states shown in Figure 4 with energies close to 6.4 eV must be the combined $3b_1 3s$ and $8b_2 3s$ Rydberg states, corresponding to the lowest ionization band reported for the PES previously.[1] The $3b_1 3s$ state, with quantum defect δ=0.864, has a lower VEE by 0.207 eV (1668 cm^{-1}). The calculated separation of the two ionic states was 0.263 eV (2121 cm^{-1}).[1] The corresponding allowed 3p-

Rydberg states, expected to lie close to 7 eV, are close to the onset of the most intense valence absorption and are discussed below.

Figure 5. Four of the highest occupied (HOMOs) and the two lowest unoccupied orbitals (LUMOs) for γ-pyrone. Many of the excitations shown in Table I feature these MOs.

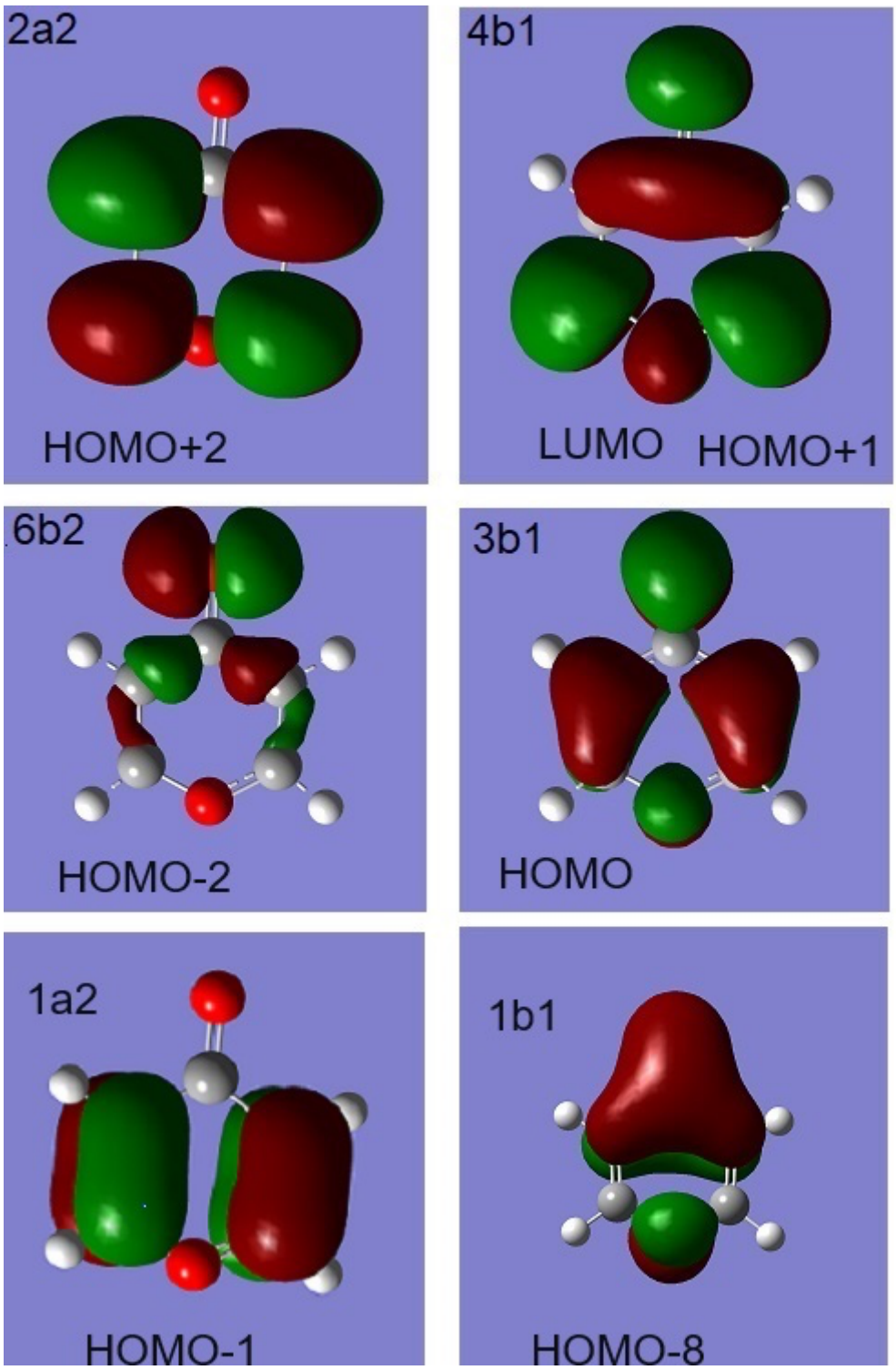

(F)The adiabatic excitation energies of γ-pyrone using the Rydberg basis.

Extrapolation of the energies for each of the 3s, 4s and 5s-Rydberg states to n = ∞, gives estimates of the vertical ionization energy with a single quantum defect (δ) by insertion in the equation: VIE - E_n = 13.61/(n - δ)^2. However, using such low quantum defects can make the extrapolated VIE unreliable. The Rydberg states, shown in Table VI, extrapolate to adiabatic ionization energies of 8.639 (303) with quantum defect 0.600(249) for $^1B_2$ and 9.410(34) eV and $^1B_1$, with standard errors in parentheses. The corresponding extrapolated energies for the p-Rydberg states are 9.511 eV ($^1B_2$) and 9.127 ($^1B_1$) and for the ionization energies of the ionic states. Although not optically allowed, the 3s, 4s and 5s-Rydberg states in $^1A_2$ symmetry can be projected to give an ionization energy value of 10.710 eV for the $^2A_2$ state, close to the observed value of 10.848 eV.[1] The corresponding set of $^1A_1$ s-Rydberg states by excitation from $8a_1$ leads to a projected ionization energy of 12.647 (163) eV; although lower than that assigned in the PES[1] at 13.25 eV, but the experimental onset is uncertain. The calculated sets of p-, d- and f-Rydberg states, and any valence states intruding in the range, are shown in Figure 4.

Table VI. The lowest calculated s- Rydberg states.

Energy / eV	Oscillator strength f(r)	Symmetry	State	Extrapolated VIE / eV
6.334	0.005	$^1B_2$	3s	8.639
7.226	0.004	$^1B_2$	4s	
8.119	0.001	$^1B_2$	5s	
6.548	0.015	$^1B_1$	3s	9.410
7.768	0.006	$^1B_1$	4s	
8.844	0.000	$^1B_1$	5s	
6.731	0.0	$^1A_2$	3s	9.043
7.757	0.0	$^1A_2$	4s	
8.435	0.0	$^1A_2$	5s	
10.215	0.009	2^1B_1	3s	12.641
11.327	0.002	2^1B_1	4s	
12.007	0.000	2^1B_1	5s	
11.377	0.014	$^1A_1$	3s	13.710
12.222	0.012	$^1A_1$	4s	

13.232	0.004	$^1A_1$	5s	

(G)The experimental UV and VUV spectrum and its analysis.

(i)The energy range up to 4.5 eV. This shows an exponential rise from 3.5 to 4.5 eV with several local maxima, as seen in black on Figure 6. The standard Boltzmann exponential function fit is shown in red, with further details of the fit in the supplementary material in SM6; while the regular residuals from this fit are in blue. The fit residuals, allow much sharper definition of the vibration frequencies, which were measured by mathematical fitting using the Origin Suite as mentioned in the supplementary material as SM7. The principal vibration frequencies are 813 and 1218 (±20) cm^{-1}.This band is usually assigned to the forbidden $^1A_2$ state, which gains intensity by mixing with the complex band starting at 4.6 eV, as discussed below.

Figure 6. The onset of the UV band, shown in black, has some poorly defined maxima. These are markedly sharpened by fitting to a Boltzmann function, as shown in red, and plotting its regular residuals, as shown in blue. The vibration frequencies from the 0-0 band, determined by electronic quadrature are 813, 1218, 1989, 3222, 4405, 5561 and 6800 cm^{-1}.

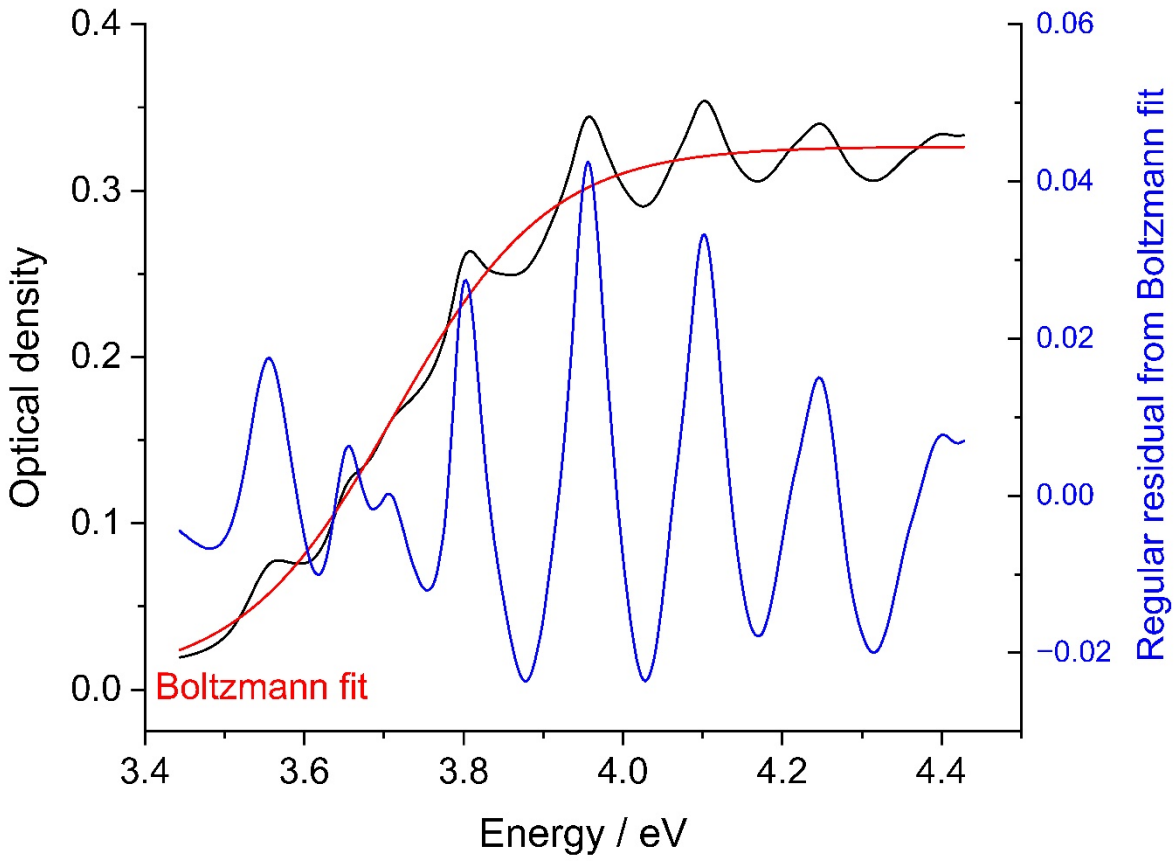

(ii) The energy range from 4.5 to 6.1 eV. This band is unusual, since it is both wide in energy, and complex in structure, with a series of undulations on the leading edge (low-energy side) up to the maximum and beyond. Fitting the spectral intensity data against a 9th order polynomial of the energy removes the broad background, and sharpens the undulations, by use of the regular residuals (in blue). These show, as in Figure 7, that the undulations are significant since many occur as very sharp peaks. Our analysis of this spectral range is shown in Figure 8. Assuming that γ-pyrone retains C_{2V} symmetry, the set of 4 low-lying states in Table I, calculated to lie in the energy range 3.9 to 5.3 eV ($^1A_2$, $^1A_1$, $^1B_2$ and $^1B_1$ in increasing energy order), create a set of overlapping (mixed) states. Since the onset of the optically forbidden $^1A_2$ state is lowest in energy, its higher vibrational members will overlap directly with the pure $^1A_1$ and $^1B_2$ states; vibronic interaction is inevitable, with $^1A_2$ gaining intensity. The high

intensity of $^1A_1$ relative to any bands in these other states, may lead to retention of some intensity in the now perturbed $^1A_1$ state. The wide range of their individual intensities in C_{2V} will lead to them all being perturbed together with the $^1A_2$ state, dominating in the linear combinations. We cannot offer a peak-by-peak analysis of the structure in Figure 8. However, the sharp but weak peak close to 4.6 eV, has the appearance of an 0-0 band followed by a vibrational manifold. Our interpretation, shown in Figure 8, makes this 0-0, the origin of the perturbed $^1B_2$ lying on top of $^1A_2$, the low intensity of the two states leading to little vibronic coupling. This is followed by overlay with the strong $^1A_1$ state, which provides intensity for the main structure. We have measured the observed peaks, and these are listed in the supplementary material as SM(A). In our analysis, the $^1B_1$ state with near zero intensity, makes no contribution to the observed profile.

Figure 7. The 4.5 to 6.0 eV region of absorption for γ-pyrone shown in black, with the regular residuals in blue after fitting to a polynomial in the energy, as discussed in the text.

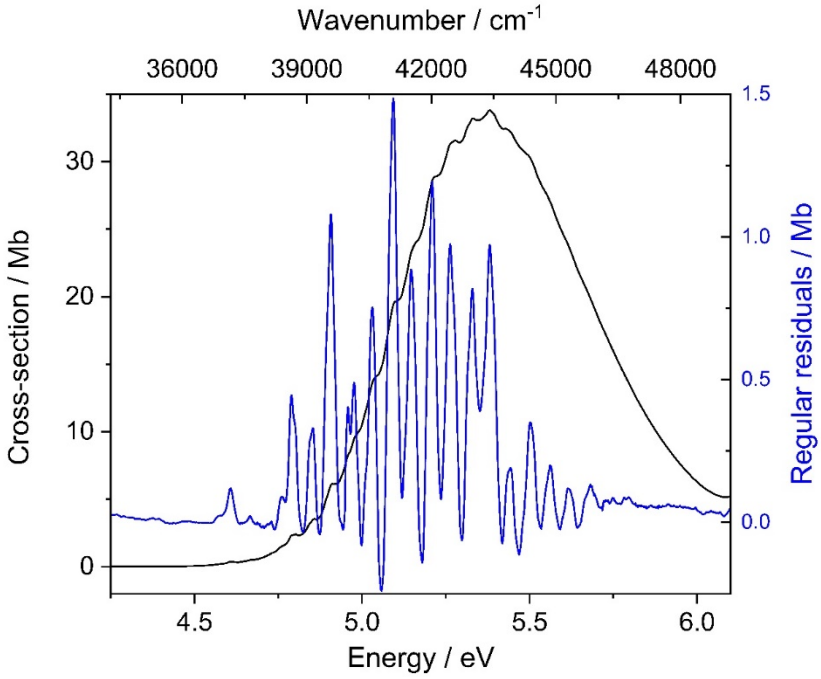

(iii)The Rydberg state region between 6.1 and 7.1 eV in the VUV spectrum.

The four lowest IE of γ-pyrone (IE_1 to IE_4) show well-defined vibrational structure with the energies (eV) shown: $^2B_1$ (9.291) as a composite band with $^2B_2$ (9.492), $^2A_2$(10.840) and 2^2B_1 (12.650 eV). Using the 3s Rydberg states based on IE_1 of γ-pyrone and a predicted δ of 0.8 we have: 6.479 ($6b_2 3s$), 7.756 ($3b_1 3s$); 9.104 ($a_2 3s$), 10.914 ($2b_1 3s$); these all lie in the energy range of the present VUV. Our recent PES analysis of the profile,[1] clearly demonstrated that the complex band for γ-pyrone between 9.2 and 9.8 eV, was for a 2-state analysis; these gains further support from the Rydberg state analysis. This agrees with the theoretical profile for s-Rydberg states in Figure 4, which also showed that none of these are predicted to lie below 6 eV. The onset of the band in the VUV spectrum at 6.348 eV corresponds to a weak peak in the PES.

Figure 8. The combined p-, d- and f-Rydberg states as determined by a combined triple zeta and polarization basis set together with each of the Rydberg functions. Thus, both valence and Rydberg functions are present in all these calculations, and the resultant roots contain both Rydberg states and low-lying valence states. One example of an intruder (valence) state lies near 9.8 eV. The calculated intensities have been increased by 0.05 units of oscillator strength to make the positions more obvious.

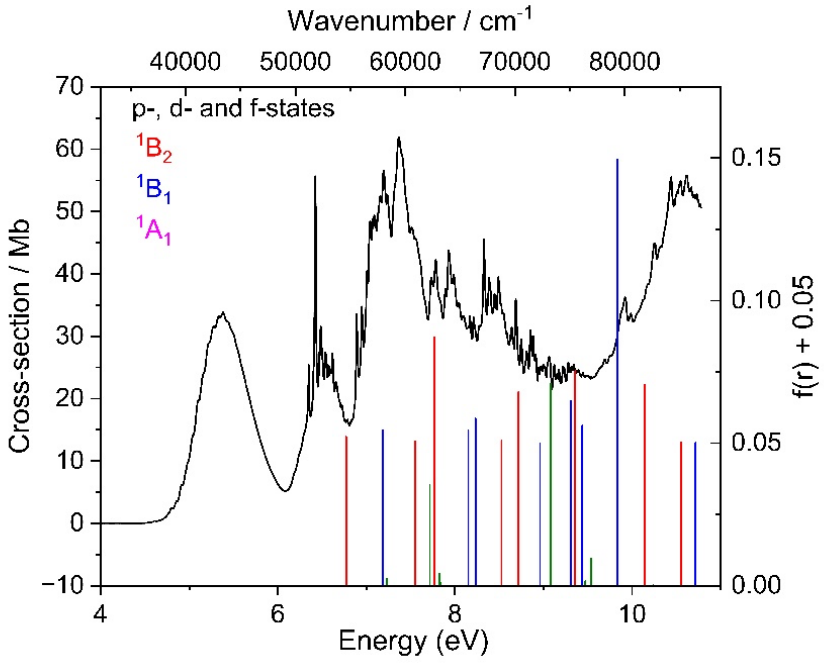

Figure 9. The VUV energy range 6.1 to 7.1 eV, shown in black, with the photoelectron spectrum (PES) reduced by 2.8669 eV (in red), and 2.3997 eV (in blue) superimposed.

Only part of the PES, the lowest energy sequence of 4-peaks occurs, which have portions of the VUV spectral profile. These correspond to the s and p Rydberg states, which have energies 6.425 and 6.89 eV, and quantum defects(δ) = 0.8212 and 0.6185 respectively, each with principal quantum number n = 3.

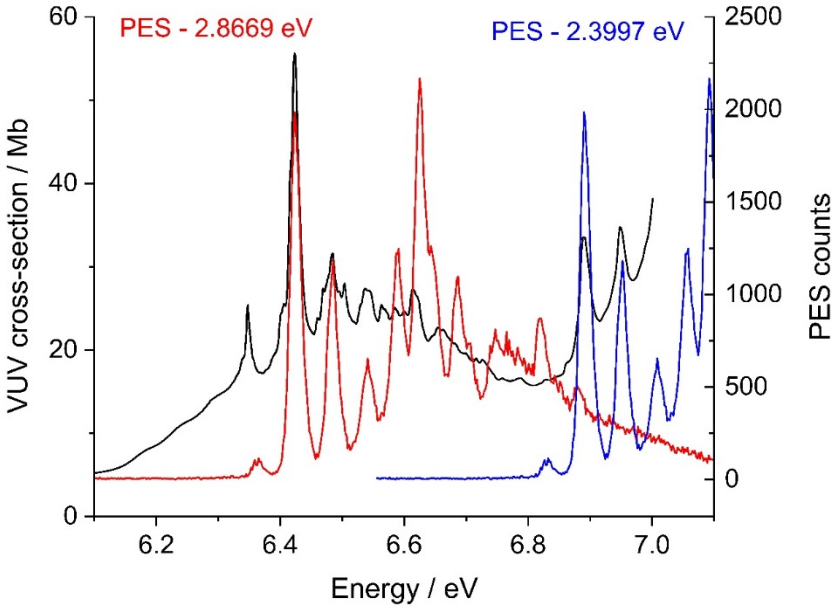

The energy range where sharp (vibrational) structure first occurs, is depicted in Figure 10, where the photoelectron spectrum is superimposed twice in blue and red, after lowering of the energy of the PES lowest ionization band by 2.867 and 2.400 eV, respectively.

(H)Assignment of the observed UV + VUV spectrum.

The experimental onset of the γ-pyrone absorption, shown in Figure 7, starts close to 4.6 eV and spreads to 6.1 eV, with a broad maximum close to 5.5 eV. The high intensity of 34 Mb is consistent at least one allowed transition under the envelope. The lowest state is of $^1A_2$ symmetry, at 3.852 eV, and is optically forbidden. The calculations, in Table I then show a set of 3 nearly degenerate allowed states under the low energy part of the UV spectrum; the second root, a $^1A_1$ state at 5.243 eV, has very high oscillator strength, but is followed by an almost degenerate $^1B_2$ state at 5.266 eV and low f(r), and then $^1B_1$ at 5.298 eV, which has accidentally zero intensity. This arises from cancellation of finite contributions to the oscillator strengths from the leading configurations ($3b_19a_1$* with $3b_18a_1$*and $3b_17a_1$*).

However, the principal cross-section under the envelope of the spectrum close to 5.4 eV must be the $^1A_1$ singlet state dominated by the ($3b_14b_1$* - $1a_22a_2$*) configurations. This onset peak clearly shows very weak undulations; these are resolved into a sharp set of peaks, by removing a broad polynomial from the data-points, with a maximum intensity of 1.48 Mb to be seen clearly, as in Figure 7. Further details are shown in the supplementary material as SM1.

Theoretical interpretation of the regular residuals superimposed on the broad spectral band shown on Figure 7, appear to require that a low intensity band occurs at the onset. The $^1A_1$ state does not appear to be consistent with this since the calculated 0-0 transition, shown in Table III, has a high intensity for both Franck-Condon and Herzberg-Teller components; neither of these components, or their combination, will fit the observed vibrational sequence shown. We are forced to conclude that the degenerate $^1B_2$ state lies lower in energy then the $^1A_1$ state, and that a 2-state interpretation is present. The tail of the $^1B_2$ then lies under the $^1A_1$ state, leading to loss of identity of both these and the even weaker $^1B_1$ state. We believe that the origin of the $^1B_2$ state is the 4.607 eV peak, which is a weak perturbation of the strong following $^1A_1$ neighbour, which leaves some of the vibrations of the $^1A_1$ state intact.

IV. CONCLUSIONS

Following our high-resolution photoelectron spectroscopy analysis of the synchrotron-based spectrum of γ-pyrone,[1] we have presented the UV and VUV absorption spectrum up to 10.78 eV (86,946 cm^{-1}) together with its analysis by density functional and configuration interaction. Both methods give close correlations to symmetry adapted coupled cluster methods. This is especially true of the CAM-B3LYP density functional in the TTDFT method when used with a triple-zeta basis which includes polarization, TZVP for example. We do not have software to perform vibrational analysis of the SAC-CI cluster wave-functions, so the close correlation of these energies with TDDFT energies strengthens confidence that these latter results will reflect the higher-level calculated excitation energy variations.

The MRD-CI method, with its second moments of the charge distribution analysis is especially suitable for differentiating between Rydberg and valence states, while the prominent level of correlation capable of incorporation within it is a powerful asset.

The UV+VUV spectrum is deceptively simple at the low energy onset. A singularly broad band, which is intense and 1.5 eV wide, is preceded by a very weak set of sharp peaks having extremely low intensity. We agree with previous analyses which assign the sharp peaks to a perturbed $^1A_2$ state, but we propose that it also includes a group of $^1A_1$, $^1B_2$ and $^1B_1$ excited states as well. The vibrational profiles of this last group of 3 states will all overlay, and mix, whereby the very varied intensities will be perturbed.

In contrast, the 6.1 to 7.5 eV region contains a set of sharp peaks superimposed on broad featureless valence states. Detailed analysis shows that these sharp states are the 3s and 3p Rydberg states leading to the lowest ionization energy X^2B_2. Comparison with the photoelectron spectrum, where overlap of the profiles of the X^2B_2 and A^2B_1 states had previously been proposed, confirms that situation. The A^2B_1 Rydberg states are absent, while the trailing vibrational structure from the X^2B_2 state is also perturbed. This situation is reminiscent of our earlier studies[46,50-52] of the mono-halogenobenzenes (C_6H_5X, where X = F, Cl, Br, and I). In that series, we found that overlap of the vibrational states from a lower lying ionic state, led to progressive broadening of the higher energy state vibrational states, the closer the two systems were placed. Thus, the normal peak width of an individual isolated peak on synchrotron-based PES, can be neatly covered by a Franck-Condon peak with a Half-Width at Half-Maximum of 70 cm^{-1}, one grossly widened may require 400 to 600 cm^{-1} to give a fit. Here in the UV-VUV, we have peaks effectively lost through broadening. The value of fitting undulating surfaces to polynomial functions to get best fits, and then plotting the regular residuals from the fits, is a powerful route to disclosing new vibrational structure.

SUPPLEMENTARY MATERIAL

See the supplementary material for additional information on each of the following: (1) Details of the theoretical methods. (a) The MRD-CI method; (b) The SAC-CI method; (c) Rydberg states. (2) (3). 2. The correlations between the symmetry adapted cluster configuration interaction, and time-dependent density functional theory and multi-reference multi-root methods. 3. Table SM3. The valence states of γ-pyrone determined by the MRD-CI method together with the TZVP basis set 4. Table SM3. The valence states of γ-pyrone determined by the MRD-CI method together with the TZVP basis set. 5. Table SM5. Adiabatic excitation energies for γ-pyrone using the CAM-B3LYP functional in the TDDFT method for (a) valence states. (b) For Rydberg states where the basis set is extended to include s-Rydberg functions; this allows both types of state to be evaluated. 7. The onset of the UV spectrum enhanced by use of a Boltzmann function, and plotting the regular residuals. 8. The electronically measured frequencies (cm^{-1}) from the 0-0 band at 28686 cm^{-1} (3.557 eV). 9. The TDDFT vertical excitation energies

ACKNOWLEDGMENTS

We thank (a) ISA, Department of Physics and Astronomy, Aarhus University for the beam time on the AU-UV beam line on ASTRID2. (b) the University of Edinburgh (Eddie3) and Edinburgh Parallel Computing Centre's (Cirrus) super-computing facilities for support; (c) numerical fitting was performed using Gnuplot-5.0.5;[53] (d) plotting used Origin 7.0;[54] (e) MOs were drawn by GaussView;[55] (f) AIM densities were evaluated using AIMQB; and T. A. Keith is thanked for provision of this software.[56]

AUTHOR DECLARATIONS

Conflict of Interest
The authors have no conflicts to disclose.

Author Contributions
Michael H. Palmer: Conceptualization (equal); Methodology (equal); Supervision (equal); Writing – original draft (equal).
Nykola C. Jones: Data curation (equal); Investigation (equal); Methodology (equal); Project administration (equal); Supervision (equal); Validation (equal).
Søren Vrønning Hoffmann: Data curation (equal); Investigation (equal); Methodology (equal); Project administration (equal); Supervision (equal); Validation (equal).
Marcello Coreno: Investigation (equal); Resources (equal).
Monica de Simone: Funding acquisition (equal); Resources (equal); Validation(equal).
Cesare Grazioli: Data curation (equal); Investigation (equal); Resources (equal); Supervision (equal).
R. Alan Aitken: Conceptualization (equal); Methodology (equal); Resources (equal); Validation (equal)
Loëlia Perrault: Methodology (equal).
Iain L. J. Patterson: Methodology (equal).

DATA AVAILABILITY

The data that support the findings of this study are available within the article and its supplementary material and available from the corresponding authors upon reasonable request.

REFERENCES

1. M. H. Palmer, M. Coreno, M. de Simone, C. Grazioli, N. C. Jones, S. Vrønning Hoffmann, R. A. Aitken, and D. K. Sonecha, "The ionic and ground states of gamma-pyrone. The photoionization spectrum studied by synchrotron radiation and interpreted by configuration interaction and density function calculations," J. Chem. Phys., **158**, 014304(2023); https://doi.org/10.1063/5.0128764.
2. H. C. Smitherman and L. N. Ferguson, "On the aromatic character of 4-pyrones," Tetrahedron, **24**, 923–932 (1968). https://doi.org/10.1016/0040-4020(68)88042-1
3. D. W. Mayo, P. J. Sapienza, R. C. Lord, and W. D. Phillips, "Exchange reactions of 4-pyrone and 4-pyrone derivatives," J. Org. Chem. **29**, 2682–2685 (1964). https://doi.org/10.1021/jo01032a049
4. C. T. Mathis and J. H. Goldstein, "Proton magnetic resonance spectra of 4-pyrone, chromone and xanthone," Spectrochim. Acta **20**, 871–878 (1964). https://doi.org/10.1016/0371-1951(64)80085-0
5. N. M. D. Brown and P. Bladon, "The proton magnetic resonance spectra of 4-pyrone, 1-thia-4-pyrone, 4-thiopyrone and 1-thia-4-thiopyrone," Spectrochim. Acta **21**, 1277–1285 (1965). https://doi.org/10.1016/0371-1951(65)80211-9
6. R. E. Mayo and J. H. Goldstein, "Proton magnetic resonance and ^{13}C–H satellite spectra of 4-pyrone: analysis and assignments," Spectrochim. Acta, Part A **23**, 55–60 (1967). https://doi.org/10.1016/0584-8539(67)80207-1
7. V. Rutar and T. C. Wong, "Utilization of the improved resolution in two-dimensional polarization transfer NMR," J. Magn. Reson. **53**, 495–499 (1983). https://doi.org/10.1016/0022-2364(83)90220-2
8. C. L. Norris, R. C. Benson, P. Beak, and W. H. Flygare, "Microwave spectrum of 2-pyrone and the molecular Zeeman effect in tropone, 2-pyrone, and 4-pyrone. Suppression of nonlocal contributions to the out-of-plane molecular magnetic susceptibilities by the insertion of a carbonyl group into an aromatic ring," J. Am. Chem. Soc. **95**, 2766–2772 (1973). https://doi.org/10.1021/ja00790a003
9. R. C. Benson, C. L. Norris, W. H. Flygare, and P. Beak, "Classification of 2- and 4-pyrone as nonaromatic on the basis of molecular magnetic susceptibility anisotropies," J. Am. Chem. Soc. **93**, 5591–5593 (1971). https://doi.org/10.1021/ja00750a055
10. J. N. MacDonald, S. A. Mackay, J. K. Tyler, A. P. Cox, and I. C. Ewart, "Microwave spectra, structures and dipole moments of 4H-pyran-4-one and its sulphur analogues," J. Chem. Soc., Faraday Trans. 2 **77**, 79–99 (1981). https://doi.org/10.1039/F29817700079
11. G. Wlodarczak, J. Demaison, B. P. Van Eijck, M. Zhao, and J. E. Boggs, "Ab initio and experimental quartic centrifugal distortion constants of acetone, pyrazole and γ-pyrone," J. Chem. Phys. **94**, 6698–6707 (1991). https://doi.org/10.1063/1.460246
12. W. H. Flygare, "Magnetic interactions in molecules and an analysis of molecular electronic charge distribution from magnetic parameters," Chem. Rev. **74**, 653–687 (1974). https://doi.org/10.1021/cr60292a003
13. J. W. Pavlik and L. T. Pauliukonis, "Photoisomerization of 4-pyrones. Nucleophilic trapping of reactive intermediates," Tetrahedron Lett., **17**, 1939–1942 (1976). https://doi.org/10.1016/S0040-4039(00)78084-1

14. S. A. Spearman and J. H. Goldstein, "An NMR study of 4-pyrone oriented in two different lyotropic mesophases," Spectrochimica Acta Part A: Molecular Spectroscopy **31**, 1565-1568 (1975). https://doi.org/10.1016/0584-8539(75)80094-8
15. D. S. Williams and T. C. Wong, "The r_α structure of partially oriented 4-pyrone determined from ^{1}H NMR spectroscopy including the ^{13}C satellites," J. Mol. Struct., **101**, 297–303 (1983). https://doi.org/10.1016/0022-2860(83)85024-8
16. A. Ligabue and P. Lazzeretti, "Theoretical determination of the magnetic properties of 2-pyrone and 4-pyrone, and *o*-benzoquinone and *p*-benzoquinone," Mol. Phys., **101**, 2497–2509 (2003). https://doi.org/10.1080/0026897031000122351
17. C. Thomson and C. Edge, "Ab initio calculations on 4H-pyran-4-one and its sulphur analogues," J. Mol. Struct., THEOCHEM, **121**, 173 (1985). https://doi.org/10.1016/0166-1280(85)80057-9
18. M. H. Palmer, N. C. Jones, S. Vronning Hoffmann, R. A. Aitken, M. Coreno, M. de Simone, C. Grazioli, and I. L. J. Patterson, "The excited states of azulene: a study of the vibrational energy levels for the lower ππ*-valence states by configuration interaction and density functional calculations, and theoretical studies of the Rydberg states," J. Chem. Phys. **157**, 154307 (2022). https://doi.org/10.1063/5.0106697
19. M. H. Palmer, S. V. Hoffmann, N. C. Jones, M. Coreno, M. de Simone, C. Grazioli, and R. A. Aitken, "The vacuum ultraviolet apsorption spectrum of norbornadiene: vibrational analysis of the singlet and triplet valence states of norbornadiene by configuration interaction and density functional calculations," J. Chem. Phys. **155**, 034308 (2021). https://doi.org/10.1063/5.0053962
20. R. D. Gordon and W. K. C. Park, "The 353 nm *n*π* transition of 4*H*-pyran-4-one and a deuterated derivative," Canadian J. Chem., **71**, 1672-1675 (1993). https://doi.org/10.1139/V93-208
21. K. Yamada, "Infrared and ultraviolet spectra of α- and γ-pyrones," Bull. Chem. Soc. Jpn. **35**, 1323-1329 (1962). https://doi.org/10.1246/bcsj.35.1323
22. N. Ishibe, H. Sugimoto, and J. B. Gallivan, "Electronic absorption and emission spectra of 4-pyrones, 4-thiopyrones and 4-pyridones," J. Chem. Soc., Faraday Trans. 2**, 71**, 1812-1822 **(**1975). https://doi.org/10.1039/F29757101812
23. N. Ishibe, M. Sunami, and M. Odani, J. Am. Chem. Soc. **95**, 463–468 (1973). https://doi.org/10.1021/ja00783a026
24. A. G. Sessions, M. P. McDonnell, D. A. Christianson, and S. Drucker, "Photoisomerization of 4*H*-pyran-4-ones to 2*H*-pyran-2-ones," J. Phys. Chem. A, **123**, 6269−6280 (2019). https://doi.org/10.1021/acs.jpca.9b04238
25. L. M. Hoffelt, M. G. Springer, and S. Drucker, "Phosphorescence excitation spectrum of the T_1 (n,π*) ← S transition of 4*H*-pyran-4-one," J. Chem. Phys. **128**, 104312 (2008) https://doi.org/10.1063/1.2834922
26. S. W. Parsons, D. G. Hucek, P. Mishra, D. F. Plusquellic, T. S. Zwier, and S. Drucker, " Jet-cooled phosphorescence excitation spectrum of the T_1 (n,π*) ← S_0 transition of 4*H*-pyran-4-one," J. Phys. Chem. A, **127**, 3636-3647(2023). https://doi.org/10.1021/acs.jpca.3c01059
27. E. R. Riegel and F. Zwilgmeyer, "Chelidonic acid," Org. Synth. **17**, 40–41 (1937). https://doi.org/10.15227/orgsyn.017.0040
28.C. De Souza, Y. Hajikarimian, and P. W. Sheldrake, "A convenient method for the preparation of pyran-4-one," Synth. Commun. **22**, 755–759 (1992). https://doi.org/10.1080/00397919208019276
29. M. H. Palmer, T. Ridley, S. V. Hoffmann, N. C. Jones, M. Coreno, M. De Simone, C. Grazioli, M. Biczysko, A. Baiardi, and P. Limao-Vieira, "Interpretation of the vacuum

ultraviolet photoabsorption spectrum of iodobenzene by *ab initio* computations," J. Chem. Phys., **142**, 134302 (2015). https://doi.org/10.1063/1.4916121
30. Gaussian 16 Revision A.03: M. J. Frisch, G. W. Trucks, H. B. Schlegel, G. E. Scuseria, M. A. Robb, J. R. Cheeseman, G. Scalmani, V. Barone, G. A. Petersson, H. Nakatsuji, X. Li, M. Caricato, A. V. Marenich, J. Bloino, B. G. Janesko, R. Gomperts, B. Mennucci, H. P. Hratchian, J. V. Ortiz, A. F. Izmaylov, J. L. Sonnenberg, D. Williams-Young, F. Ding, F. Lipparini, F. Egidi, J. Goings, B. Peng, A. Petrone, T. Henderson, D. Ranasinghe, V. G. Zakrzewski, J. Gao, N. Rega, G. Zheng, W. Liang, M. Hada, M. Ehara, K. Toyota, R. Fukuda, J. Hasegawa, M. Ishida, T. Nakajim,a Y. Honda, O. Kitao, H. Nakai, T. Vreven, K. Throssell, J. A. Montgomery Jr,. J. E. Peralta, F. Ogliaro, M. J. Bearpark, J. J. Heyd, E. N. Brothers, K. N. Kudin, V. N. Staroverov, T. A. Keith, R. Kobayashi, J. Normand, K. Raghavachari, A. P. Rendell, J. C. Burant, S. S. Iyengar, J. Tomasi, M. Cossi, J. M. Millam, M. Klene, C. Adamo, R. Cammi, J. W. Ochterski, R. L. Martin, K. Morokuma, O. Farkas, J. B. Foresman and D. J. Fox Gaussian Inc. Wallingford CT 2016.
31. H. Nakatsuji and K. Hirao, "Cluster expansion of the wave function. Electron correlations in singlet and triplet excited states, ionized states, and electron attached states by SAC and SAC-CI theories," Int. J. Quantum Chem. **20**, 1301–1313 (1981). https://doi.org/10.1002/qua.560200613
32. H. Nakatsuji and T. Yonezawa, "Cluster expansion of the wave function. Satellite peaks of the inner-valence ionization of H_2O studied by the SAC and SAC CI theories," Chem. Phys. Lett. **87**, 426–431 (1982). https://doi.org/10.1016/0009-2614(82)83004-2
33. H. Nakatsuji, "Cluster expansion of the wavefunction, valence and rydberg excitations, ionizations, and inner-valence ionizations of CO_2 and N_2O studied by the sac and sac CI theories," Chem. Phys. **75**, 425–441 (1983). https://doi.org/10.1016/0301-0104(83)85209-4
34. H. Nakatsuji, "Cluster expansion of the wave function. Ionization and excitation spectra of NO radical studied by the SAC and SAC-CI theory," Int. J. Quantum Chem. Symp. **24** (S17), 241–255 (1983). https://doi.org/10.1002/qua.560240830
35. H. Nakatsuji, K. Ohta, and T. Yonezawa, "Cluster expansion of the wave function. Spin and electron correlations in doublet radicals studied by the symmetry adapted cluster and symmetry adapted cluster-configuration interaction theories," J. Phys. Chem. **87**, 3068–3074 (1983). https://doi.org/10.1021/j100239a022
36.V. Barone, J. Bloino, M. Biczysko, and F. Santoro, "Fully integrated approach to compute vibrationally resolved optical spectra: from small molecules to macrosystems," J. Chem. Theory Comput. **5**, 540–554 (2009). https://doi.org/10.1021/ct8004744
37. J. Bloino, M. Biczysko, F. Santoro, and V. Barone, "General apprioach to compute vibrationally resolved one-photon electronic spectra," J. Chem. Theory Comput. **6**, 1256–1274 (2010). https://doi.org/10.1021/ct9006772
38. A. Baiardi, J. Bloino, and V. Barone, "General time dependent approach to vibronic spectroscopy including Franck-Condon, Herzberg-Teller, and Duschinsky effects," J. Chem. Theory Comput. **9**, 4097–4115 (2013). https://doi.org/10.1021/ct400450k
39. P. Hohenberg and W. Kohn, "Inhomogeneous electron gas," Phys. Rev. **136**, B864–B871 (1964). https://doi.org/10.1103/PhysRev.136.B864
40. W. Kohn and L. J. Sham, "Self-consistent equations including exchange and correlation effects," Phys. Rev. **140**, A1133–A1138 (1965). https://doi.org/10.1103/PhysRev.140.A1133
41. R. G. Parr and W. Yang, Density-Functional Theory of Atoms and Molecules, Oxford University Press, Oxford, 1989.
42. A. D. Becke, "Density-functional thermochemistry III. The role of exact exchange," J. Chem. Phys. **98**, 5648–5652 (1993). https://doi.org/10.1063/1.464913

43. T. Yanai, D. P. Tew, and N. C. Handy, "A new hybrid exchange-correlation functional using the Coulomb-attenuating method (CAM-B3LYP)," Chem. Phys. Lett. **393**, 51–57 (2004). https://doi.org/10.1016/j.cplett.2004.06.011
44. R. J. Buenker and S. Krebs, "The configuration-driven approach for multireference configuration interaction calculations," in Recent Advances in Multireference Methods, Recent Advances in Computational Chemistry Vol. 4 (World Scientific, 1999), pp. 1–29. https://doi.org/10.1142/9789812812186_0001
45. M. F. Guest, I. J. Bush, H. J. J. Van Dam, P. Sherwood, J. M. H. Thomas, J. H. Van Lenthe, R. W. A. Havenith, and J. Kendrick, "The GAMESS-UK electronic structurepackage: algorithms, developments and applications," Mol. Phys. **103**, 719–747 (2005). https://doi.org/10.1080/00268970512331340592
46. M. H. Palmer, S. Vrønning Hoffmann, N. C. Jones, M. Coreno, M. de Simone, C. Grazioli, R. A. Aitken, and C. Peureux. "High-level studies of the singlet states of quadricyclane including analysis of a new experimental vacuum ultraviolet absorption spectrum by configuration interaction and density functional calculations," J. Chem. Phys. **158**, 234303 (2023). https://doi.org/10.1063/5.0151758
47. M. J. Frisch, J. A. Pople, and J. S. Binkley, "Self-consistent molecular orbital methods 25. Supplementary functions for Gaussian basis sets," J. Chem. Phys., **80** 3265-3269 (1984). https://doi.org/10.1063/1.447079
48. R. Ahlrichs and P.R. Taylor, "The choice of Gaussian basis sets for molecular electronic structure calculations," J. Chim. Phys., **78**, 315-324 (1981). https://doi.org/10.1051/jcp/1981780315
49.(a) R. Fausto, G. Quinteiro, and S. Breda, "Vibrational spectroscopy and ab initio MO study of the molecular structure and vibrational spectra of α- and γ-pyrones," J. Mol. Struct., **598**, 287-303 (2001). https://doi.org/10.1016/S0022-2860(01)00639-1. (b) J. Seixas de Melo, G. Quinteiro, J. Pina, S. Breda, and R. Fausto, "Spectroscopic characterization of α- and γ-pyrones and their substituted 4-hydroxy and 4-methoxy derivatives: an integrated infrared, photophysical and theoretical study," J. Mol. Struct., **565-566**, 59-67 (2001) https://doi.org/10.1016/S0022-2860(00)00944-3
50. M. H. Palmer, T.Ridley, S. Vronning Hoffmann, N. C. Jones, M. Coreno, M. de Simone, C.Grazioli, Teng Zhang, M. Biczysko, A. Baiardi, and K. A. Petersen, "Combined theoretical and experimental study of the valence, Rydberg, and ionic states of chlorobenzene," J. Chem. Phys. **144**, 124302 (2016). https://doi.org/10.1063/1.4944078
51. M. H. Palmer, T. Ridley, S. Vrønning Hoffmann, N. C. Jones, M. Coreno, M. de Simone, C. Grazioli, Teng Zhang, M. Biczysko, A. Baiardi, and K. Peterson, "Interpretation of the photoelectron, ultraviolet, and vacuum ultraviolet photoabsorption spectra of bromobenzene by *ab initio* configuration interaction and DFT computations," J. Chem. Phys. **143**, 154303 (2015). https://doi.org/10.1063/1.4933419.
52. M. H. Palmer, T. Ridley, S. Vronning Hoffmann, N. C. Jones, M. Coreno, M. de Simone, C. Grazioli, Teng Zhang, M. Biczysko, A. Baiardi, and K. A. Petersen, "Combined theoretical and experimental study of the valence, Rydberg, and ionic states of fluorobenzene," J. Chem. Phys. **144**, 204305 (2016). https://doi.org/10.1063/1.4949548
53.See http://www.gnuplot.info/ for Gnuplot Release 5.0.7.
54.Origin Version 2019, OriginLab Corporation, Northampton, MA, USA, 2019s.
55. R. Dennington, T. A. Keith, and J. M. Millam, GaussView, Version 6.1, Semichem Inc., Shawnee Mission, KS, 2016.
56. T. A. Keith, AIMQB (Version 14.11.23, Standard), T. K. Gristmill Software, Overland Park, KS, 2017, www.aim.tkgristmill.com.